mathematics

MDPI

Article

Design of Continuous Finite-Time Controller Based on Adaptive Tuning Approach for Disturbed Boost Converters

Hammad Alnuman [1], Kuo-Hsien Hsia [2], Mohammadreza Askari Sepestanaki [3], Emad M. Ahmed [1], Saleh Mobayen [3,*] and Ammar Armghan [1,*]

[1] Department of Electrical Engineering, College of Engineering, Jouf University, Sakaka 72388, Saudi Arabia
[2] Department of Electrical Engineering, National Yunlin University of Science and Technology, 123 University Road, Douliou 64002, Taiwan
[3] Graduate School of Intelligent Data Science, National Yunlin University of Science and Technology, 123 University Road, Section 3, Douliou 640301, Taiwan
* Correspondence: aarmghan@ju.edu.sa (A.A.); mobayens@yuntech.edu.tw (S.M.)

Abstract: This research study proposes a continuous finite-time controller based on the adaptive tuning approach for the boost converters with unknown disturbances. A Lyapunov candidate function which contains an absolute function based on the fractional power of the sliding surface is employed to attain a smooth continuous control input. The recommended technique can eliminate the chattering phenomenon made by the sliding mode control signal and improve the control performance. Furthermore, the continuous adaptive-tuning control law is given to estimate the unknown bounds of exterior disturbances. The performance of the adaptive-tuned terminal sliding mode control law to the load variations and parametric uncertainties, and the input voltage, are studied in the MATLAB-Simulink environment. The obtained simulation results confirm the effectiveness of the suggested technique.

Keywords: DC–DC boost converter; sliding mode control; Lyapunov function; adaptive control; external disturbances

MSC: 93D09; 93D30; 93D40; 93D21; 93C40; 62F35

check for updates

Citation: Alnuman, H.; Hsia, K.-H.; Sepestanaki, M.A.; Ahmed, E.M.; Mobayen, S.; Armghan, A. Design of Continuous Finite-Time Controller Based on Adaptive Tuning Approach for Disturbed Boost Converters. *Mathematics* **2023**, *11*, 1757. https://doi.org/10.3390/math11071757

Academic Editors: António Lopes and Aydin Azizi

Received: 8 March 2023
Revised: 30 March 2023
Accepted: 5 April 2023
Published: 6 April 2023

Copyright: © 2023 by the authors. Licensee MDPI, Basel, Switzerland. This article is an open access article distributed under the terms and conditions of the Creative Commons Attribution (CC BY) license (https://creativecommons.org/licenses/by/4.0/).

1. Introduction

A microgrid consists of various sources of small power generation, which makes it very flexible and efficient. It connects the utility generation units and the local grid through the inverter and prevents power outages [1–3]. However, electrical power systems are experiencing increased load due to increased power demand and limited power availability [4,5]. The primary challenges for companies are to ensure the stability, security, and reliability of the network and optimize energy efficiency [6]. Most conventional energy sources cause environmental pollution and increase the cost of production. These reasons support the search for alternative energy, which causes an exponential increase in the use of renewable energy sources. Renewable energy systems are integrated with the grid using power electronic converters supported by high-performance controllers [7]. Today, the widespread application of DC–DC power electronic converters in renewable energy sources, electric vehicles, emergency power supplies, and microgrids is undeniable.

The most important task of buck–boost converters is to increase/decrease the input voltage with simple circuits and control loops [8]. However, the voltage gain is bounded by the inverse output voltage [9,10]. Because of representing non-minimum phase behaviour due to right half-plane zero and nonlinear dynamics, designing a controller for DC–DC converters is much more challenging compared to buck converters [11–14]. Various control methods have been proposed for DC–DC boost converter systems, including the feedforward control methods [15,16], proportional-integral-derivative (PID) control method [17,18],

predictive control [19,20], fuzzy controller techniques [21,22], optimal control [23,24], adaptive control [25,26], sliding mode control (SMC) [27–29], neural networks [30], and robust time-delay control method [31].

Among the mentioned control methods for the DC–DC boost converter (DBC), the SMC technique is effective and applicable for nonlinear systems and has strong robustness against parameter uncertainty and external disturbances [32,33]. In Refs. [28,34], the classical SMC technique is designed for the boost converter system. However, the most critical weakness of the typical sliding mode controller is the chattering phenomenon, because the chattering problem reduces the accuracy of the controller and increases the oscillation in the system [35]. Using the saturation function or tangent hyperbolic instead of the discontinuous sign function is one of the ways to reduce the chattering, which also positively affects the controller's performance [36–38]. In Refs. [39,40], other second-order SMC and super-twisting SMC techniques have been used for DC–DC converters. Knowing the upper boundaries of the disturbance derivatives is one requirement for designing and implementing these controllers. In conventional SMC methods, the switching gain causes chattering problems. An adaptive sliding mode control (ASMC) technique is considered in Ref. [1] as an effective technique to overcome the chattering in DC–DC converters when the upper bound of the disturbance derivative is unknown.

Recent research has considered a finite-time control method called terminal sliding mode control (TSMC). In the conventional SMC method, the state trajectories of the system are not robust to uncertainties in the phase of converging the sliding surface, and the system states reach the origin in the infinite time; however, in the TSMC method, the system state trajectories converge to the origin in a finite time due to the nonlinearity of the sliding surface [41]. In Ref. [42], a fractional high-order ATSMC for the nonlinear robotic manipulator with alternating loads is provided. In Ref. [43], an ATSMC scheme with finite-time stability and robustness to uncertainties is proposed to stabilize the chaotic systems. The reference [44] proposed a fixed-time SMC scheme for the rapid and accurate trajectory tracking of a fully actuated unmanned surface vehicle (USV) in the presence of model uncertainties and external disturbances. The proposed fixed-time SMC scheme can guarantee that the position and velocity tracking errors converge to zero in fixed time with strong robustness against lumped uncertainties. In Ref. [45], a fractional-order TSMC law with a fractional-order switching surface is presented to synchronize two dissimilar uncertain chaotic systems in a finite time; however, in this approach, the upper boundaries of unknown disturbances are known.

To the best of the author's knowledge, very few attempts have been made to propose an adaptive robust TSMC approach for disturbed boost converter systems which can completely eliminate the discontinuity in the control laws. In this paper, we propose a novel technique to prevent the chattering phenomenon in TSMC. We combine the concepts of finite-time stability and disturbance observer to achieve a finite-time observer for boost converter systems in the presence of the external disturbances and white noise. The planned control approach proposes a new candidate Lyapunov function including an absolute fractional power function of the switching surface, where the designed controller is continuous and smooth. This technique completely eliminates the chattering phenomenon caused by the switching law and ensures the high-accuracy performance. A new parameter-tuning adaptive control scheme is designed to estimate the unknown disturbance boundary. The proposed control strategy has the following advantages over the existing methods:

- A novel adaptive continuous finite-time controller is designed for disturbed boost converter systems in the presence of white noise and model uncertainty;
- A design method which guarantees the convergence and maintenance of the system state trajectories to a predefined neighbourhood of the origin in the finite time;
- Estimating the disturbance boundaries using an adaptive continuous scheme to adjust the controller adaptation gain;
- Eliminating the chattering phenomenon using a switching function based on a continuous adaptation gain.

The structure of this article is organized as follows: Section 2 examines the state-space modelling of the dynamics of DBC systems. The ACTSMC strategy is presented in Section 3. Section 4 presents the simulation results. Finally, Section 5 is devoted to the conclusions.

2. DC–DC Boost Converter

The DC–DC converter is an electronic circuit that produces a continuous, variable source from a constant, continuous source. These converters generally include a switch (S_ω) with control input u between 0 and 1, a fast diode D, and components R, L, C. To design the controller, the mathematical model of these converters must be presented, which is obtained by applying Kirchhoff's two laws (current and voltage). As shown in Figure 1, a DBC increases the output voltage relative to the input voltage.

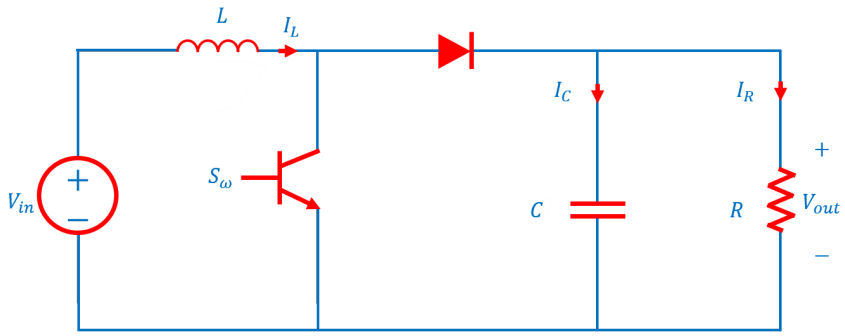

Figure 1. DC–DC boost converter.

The state-space model when the switch is on is as follows:

$$V_{in} = V_L \rightarrow V_L = L\frac{dI_L}{dt} \rightarrow \dot{I}_L = \frac{1}{L}(V_{in})\ I_c = I_R \rightarrow V_{out} = V_C \rightarrow I_c = C\frac{dV_C}{dt} \rightarrow \dot{V}_{out} = \frac{1}{C}\left(\frac{V_{out}}{R}\right), \tag{1}$$

when the key is off, the following relationship is obtained:

$$\dot{I}_L = \frac{1}{L}(V_{in} - V_{out})\dot{V}_{out} = \frac{1}{C}\left(I_L - \frac{V_{out}}{R}\right). \tag{2}$$

By selecting output voltage V_{out} and inductor current I_L as system state variables, the following relationship will be obtained:

$$x_1 = I_L x_2 = V_{out}. \tag{3}$$

As a result, the state-space equations of the DBC system are obtained as follows:

$$\dot{x}_1 = \frac{(V_i - x_1)}{L} + \frac{x_2}{L}u\dot{x}_2 = \frac{1}{C}\left(x_1 - \frac{x_2}{R}\right) - \frac{x_2}{C}u. \tag{4}$$

In the following, to simplify the calculations, the following equations are defined.

$$g_1(x) = \frac{(V_i - x_1)}{L}, \quad a_1(x) = \frac{x_2}{L}g_2(x) = \frac{1}{C}\left(x_1 - \frac{x_2}{R}\right), \quad a_2(x) = \frac{x_2}{C}. \tag{5}$$

Lemma 1 [41]**.** *Consider $x \in \mathcal{Y} \subset R^n$ and $\dot{x} = \Theta(x), \Theta : R^n \rightarrow R^n$ as a continuous system, in the region $\mathcal{Y}$ as the open neighborhood of origin and locally Lipschitz at $\mathcal{Y}\{0\}$ and $\Theta(0) = 0$. Moreover, assume that the following conditions hold, if there is a continuous Lyapunov function $V : \mathcal{Y} \rightarrow R$:*

(a) V is positive-definite;
(b) time derivative of V at $\mathcal{Y}\{0\}$ is negative-definite;
(c) There are positive real values m and $0 < a < 1$, and a neighbourhood $\mathcal{N} \subset \mathcal{Y}$ of origin such that:

$$\dot{V} + mV^a \leq 0. \tag{6}$$

The system $\dot{x} = \theta(x)$ at $\dot{x} = \theta(x)$ has a stable finite-time equilibrium point at the origin.

According to Lemma 1, the Lyapunov function $V : \aleph \to R$ tends to zero in a finite time for the initial time t_0. Therefore, the following settling time is obtained:

$$t_s = t_0 + \frac{V^{1-a}(t_0)}{\pounds(1-a)} \tag{7}$$

where £ represents a positive constant coefficient and t_s represents the system's settling time.

3. Control Design

In this segment, a developed ATSMC strategy is planned for the DBC. The primary target of the new ATSMC technique is to present a strategy such that the chattering problem is eliminated.

Consider the DBC system under unknown external disturbances as follows:

$$\dot{x}_i(t) = g_i(x) + a_i(x)u(t) + d(x_i(t), t), \tag{8}$$

where $x_i(t) = \begin{bmatrix} x_1(t) & x_2(t) \end{bmatrix}^T$ is the DC–DC boost converter's state; $u(t)$ is the control input; $d_i(x_i(t), t)$ is the unknown external disturbances but bounded as $|d(x_i(t), t)| < D$; and $g_i(x)$ and $a_i(x)$ introduced in relation (5) are the desired references.

The DBC (8) is supposed to trace the reference $\widetilde{x}(t)$. The error function is as follows

$$e(t) = x_1(t) - \widetilde{x}_1(t), \tag{9}$$

where $x_i(t) = I_L$ is the DC–DC boost converter's state, and $\widetilde{x}_1(t) = \frac{{V_{out}}^2}{RV_{in}}$ is the desired reference. In the following, the sliding surface is considered as follows:

$$\tau(t) = \rho e(t), \tag{10}$$

where ρ represents a positive and constant parameter to satisfy the stability of the closed-loop system when the DBC state trajectories attain the switching surface.

Now, an SMC law is designed using the Lyapunov stability law for the DBC system, so the designed control law is smooth and continues and eliminates the chattering phenomenon.

$$u = {a_1}^{-1}\left(\dot{\widetilde{x}}_1(t) - \frac{\sigma z}{\eta s}\tau(t)^{b+1-\frac{s}{z}} - g_1(x)\right), \tag{11}$$

where η and σ are positive parameters to regulate the speed of the converging to the switching surface; z and s are positive odd integers with condition $z > s$; b signifies the positive odd integer.

The candidate Lyapunov function is considered to prove the stability of the closed-loop DBC system:

$$V = \eta|\tau(t)|^{\frac{s}{z}} = \eta\tau(t)^{\frac{s}{z}} sgn\left(\tau(t)^{\frac{s}{z}}\right) = \eta\tau(t)^{\frac{s}{z}} sgn(\tau(t)). \tag{12}$$

The first step after introducing the candidate Lyapunov function is to take its time derivative as follows:

$$\dot{V} = \eta\frac{s}{z}\tau(t)^{\frac{s}{z}-1}\dot{\tau}(t) sgn(\tau(t)). \tag{13}$$

The stability of the system is proven when the condition $\dot{V}(t) < 0$ is satisfied, as a result, we have:

$$\dot{V} = -\eta|\tau(t)|^b = -\eta\tau(t)^b sgn(\tau(t)) < 0. \tag{14}$$

By applying (13) and (14), the following relation will be obtained:

$$\dot{\tau}_i = -\frac{\sigma z}{\eta s}\tau(t)^{b+1-\frac{s}{z}}. \tag{15}$$

By subsisting the time-derivative of sliding surface (10) into (15), the following is obtained:

$$\rho_i \dot{e}_i(t) = -\frac{\sigma z}{\eta s}\tau(t)^{b+1-\frac{s}{z}}. \tag{16}$$

Then, by using (8), (9), and (16), the controller is obtained as (10). Now, by subsisting (11) into (13), we have:

$$\dot{V}(t) = \eta\frac{s}{z}\tau(t)^{\frac{s}{z}-1}sgn(\tau(t)) \times \left(d(x_i(t),t) - \frac{\sigma z}{\eta s}\tau(t)^{b+1-\frac{s}{z}}\right), \tag{17}$$

where because $\tau(t)^{\frac{s}{z}-1}sgn(\tau(t)) > 0$ and $\dot{V}(t) < 0$ (to ensure stability), the following inequality should be met:

$$d(x_i(t),t) - \frac{\sigma z}{\eta s}\tau(t)^{b+1-\frac{s}{z}} \leq 0, \tag{18}$$

or equivalent,

$$\sigma \geq \frac{\eta s D}{z}\tau(t)^{\frac{s}{z}-b-1}. \tag{19}$$

Equation (19) shows that the amplitude of the sliding surface changes directly with the changes in the μ amplitude. According to this point, $\sigma \geq \varphi|\tau(t)|^{\alpha}$ is considered the boundary of μ changes, where α represents the changes of the sliding surface and φ represents the constant coefficient. The strong stability of the DBC system is satisfied based on Equation (19).

Finding the appropriate parameter D is difficult due to the unknown upper bounds of external disturbances. As a result, to approximate the unknown upper bound of the external disturbances, the TSMC is combined with the continuous adaptive controller.

Theorem 1. *Consider the DBC (8) and switching surface (10). Suppose that disturbance $d(x_i(t),t)$ is unknown, but bounded with $|d(x_i(t),t)| < D$. Assume $\hat{D}$ as the estimation of D, which is adapted as*

$$\dot{\hat{D}} = \mu|\tau(t)|^{\frac{s}{z}-1}, \tag{20}$$

where μ is a positive constant; s and z specify two positive odd integers with $s > n$, applying the adaptive controller as

$$u = {a_1}^{-1}\left(\dot{\tilde{x}}_1(t) - \frac{\sigma s}{\eta z}\tau(t)^{b+1-\frac{s}{z}} - g_1(x) - \hat{D}(t)\right), \tag{21}$$

where σ_i is a scalar value. Then, the DBC state trajectories (8) are converged to the sliding surface (10) in the finite time.

Proof. Consider a positive definite candidate Lyapunov function as follows:

$$V(t) = \eta\tau(t)^{\frac{s}{z}}sgn(\tau(t)) + 0.5\vartheta\widetilde{D}(t)^2, \tag{22}$$

where $\widetilde{D}(t) = \hat{D}(t) - D(t)$ and $0 < \vartheta < \frac{\sigma n}{\eta m}$. Then, $\dot{V}(t)$ is calculated by utilizing Equations (10) and (20):

$$\dot{V}(t) = \frac{\eta s}{z}\tau(t)^{\frac{s}{z}-1}\dot{\tau}(t)sgn(\tau(t)) + \vartheta\widetilde{D}(t)\dot{\widetilde{D}}(t) = \frac{\eta s}{z}\tau(t)^{\frac{s}{z}-1} \times \left(\rho\dot{e}(t)\right)sgn(\tau(t)) + \vartheta\mu\widetilde{D}(t)|\tau(t)|^{\frac{s}{z}-1}. \tag{23}$$

From (8), (9), and (23), it can be concluded that

$$\dot{V}(t) = \frac{\eta s}{z}\tau(t)^{\frac{s}{z}-1} \times \left(\rho(g_1(x) + a_1(x)u(t) + d(x_i(t),t)) - \rho\dot{\widetilde{x}}_1(t)\right)sgn(\tau(t)) + \vartheta\mu\left(\hat{D}(t) - D(t)\right)|\tau(t)|^{\frac{s}{z}-1}. \tag{24}$$

Substituting (21) into (24) gives the result

$$\dot{V}(t) = \frac{\eta s}{z}d(x_i(t),t)|\tau(t)|^{\frac{s}{z}-1} - \sigma|\tau(t)|^b - \frac{\eta s}{z}\hat{D}(t)|\tau(t)|^{\frac{s}{z}-1} + \vartheta\mu\left(\hat{D}(t) - D(t)\right)|\tau(t)|^{\frac{s}{z}-1}. \tag{25}$$

Equation (25) can be rewritten as follows:

$$\begin{aligned}\dot{V}(t) &\le \tfrac{\eta s}{z}d(x_i(t),t)|\tau(t)|^{\frac{s}{z}-1} - \tfrac{\eta s}{z}\hat{D}(t)|\tau(t)|^{\frac{s}{z}-1} + \tfrac{\eta s}{z}\left(\hat{D}(t) - D(t)\right)|\tau(t)|^{\frac{s}{z}-1} \\ &\quad + \vartheta\mu\widetilde{D}(t)|\tau(t)|^{\frac{s}{z}-1} \\ &\le -\tfrac{\eta s}{z}(D(t) - d(x_i(t),t))|\tau(t)|^{\frac{s}{z}-1} - \left(\tfrac{\eta s}{z} - \vartheta\mu\right)\widetilde{D}(t)|\tau(t)|^{\frac{s}{z}-1}.\end{aligned} \tag{26}$$

Insomuch $d(x_i(t),t) < D(t)$ and $\vartheta\mu < \frac{\eta s}{z}$, then, the following relation is obtained:

$$\begin{aligned}\dot{V}(t) &\le \tfrac{s\sqrt{\eta}}{z}(D(t) - d(x_i(t),t))|\tau(t)|^{\frac{s}{2z}-1}\left(\sqrt{\eta}|\tau(t)|^{\frac{s}{2z}}\right) \\ &\quad -\sqrt{\tfrac{2}{\vartheta}}\left(\tfrac{\eta s}{z} - \vartheta\mu\right)|\tau(t)|^{\frac{s}{2z}-1}\left(\sqrt{\tfrac{\vartheta}{2}}\widetilde{D}(t)\right) \\ &\le -\min\left\{\tfrac{s\sqrt{\eta}}{z}(D(t) - d(x_i(t),t))|\tau(t)|^{\frac{s}{2z}-1}, \sqrt{\tfrac{2}{\vartheta}}\left(\tfrac{\eta s}{z} - \vartheta\mu\right)|\tau(t)|^{\frac{s}{z}-1}\right\} \\ &\quad \times\left(\sqrt{\eta}|\tau(t)|^{\frac{s}{2z}} + \sqrt{\tfrac{\vartheta}{2}}\widetilde{D}(t)\right) = -\omega V(t)^{0.5},\end{aligned} \tag{27}$$

where $\omega = \left\{\frac{s\sqrt{\eta}}{z}(D(t) - d(x_i(t),t))|\tau(t)|^{\frac{s}{2z}-1}, \sqrt{\frac{2}{\vartheta}}\left(\frac{\eta s}{z} - \vartheta\mu\right)|\tau(t)|^{\frac{s}{z}-1}\right\} > 0$. Finally, based on Lemma 1, by considering the adaptive controller (24), the state trajectories of DBC (8) reach surface $\tau = 0$ in the finite time. □

Remark 1. *According to Equation (21), it can be seen the proposed control strategy gives approaches to remove the chattering problem because no signum function is used in (21). In consequence, the presented control low is smooth and continuous. The block diagram of the ACTSMC system is represented in Figure 2.*

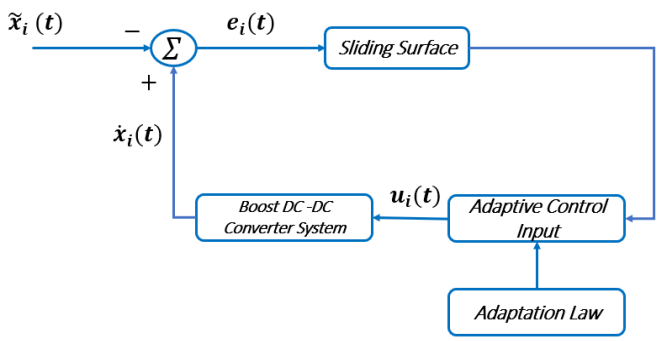

Figure 2. Block diagram of the ACTSMC system.

4. Simulation Results

In what follows, the state-space relationship of the DBC system is considered as the following:

$$\dot{x}_i(t) = g_i(x) + a_i(x)u(t) + d(x_i(t),t),$$

where $x_i(t) = \begin{bmatrix} x_1(t) & x_2(t) \end{bmatrix}^T$ is the DC–DC boost converter's state; $u(t)$ is the control input; $d(x_i(t), t)$ is the unknown disturbances but bounded as $|d(x_i(t), t)| < D$; and $g_i(x)$ and $a_i(x)$ introduced in relation (5) are the desired references.

Moreover, the DBC parameters used in the simulation examples are $L = 10$ mH, $C = 100$ µF, $R = 30\ \Omega$, $V_{out} = 40$ V, and $V_{in} = 12$ V. The external disturbance of the DBC system are considered as $d(x_i(t), t) = \cos\left(\frac{\pi t}{3}\right)$ and $\mu = \rho = 1$. In addition, simulations have been carried out in four scenarios to show the efficiency and effectiveness of the proposed control method against uncertainties and external disturbances.

Scenario 1. *In the first step, the DBC system parameters are assumed as $V_{in} = 12$ V, $V_{out} = 40$ V, and $R = 30\ \Omega$. Now, the responses of the DBC system are compared with another method in terms of speed of convergence and robustness, as well as the elimination of the chattering phenomenon. Reference* [1] *has used an ASMC for a novel buck–boost converter based on a Zeta converter. The DBC system is simulated in MATLAB-Simulink software.* Figure 3 *demonstrates the comparison of the behaviour of the inductor current and the output voltage, based on which the proposed controller performs well in terms of convergence rate and elimination of the chattering problem and has less overshoot and undershoot than the method in Ref.* [1]. *The control effort signals are also displayed in* Figure 4, *demonstrating that the control input signals are smooth and have no chattering.* Figure 5 *shows the sliding surface, indicating that the control input's amplitude is appropriate. The adaptation gain is also demonstrated in* Figure 6, *based on which it can be seen that the external disturbances are well estimated by the proposed controller.*

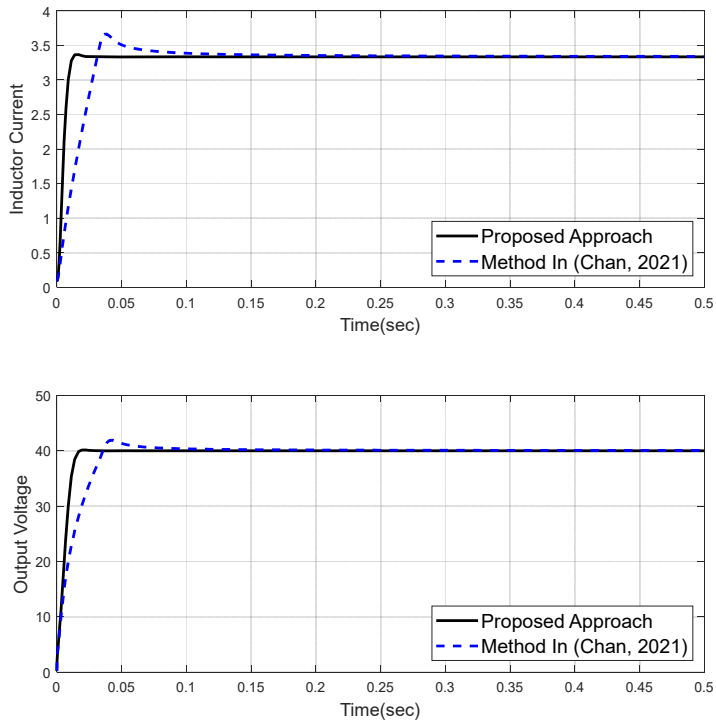

Figure 3. Comparison of the behaviour of the inductor current and output voltage with the results of the method in Ref. [1].

According to the obtained simulation results in Figures 3–6 and Table 1, it can be seen that the inductor current and output voltage of the DBC system are shown in Figure 3, which converges to the $\tilde{x}_1(t)$ after a short period of time; additionally, the suggested controller technique has a lower amount of overshoot and undershoot compared to the method in Ref. [1]. Based on Table 1 and Figure 4, the control effort signal in the proposed method successfully removes the chattering problem and has better results than the method in Ref. [1] in the steady state.

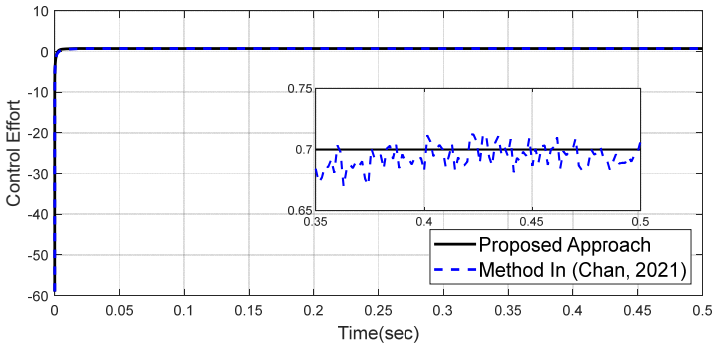

Figure 4. Controller effort signals [1].

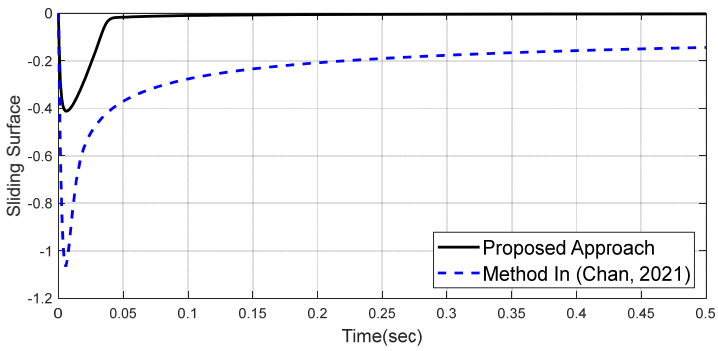

Figure 5. Sliding surfaces [1].

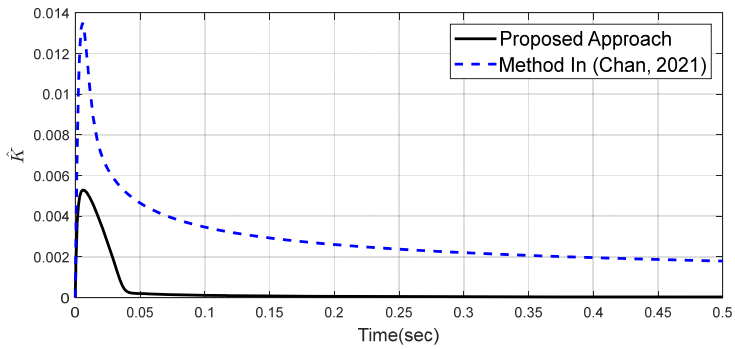

Figure 6. Adaptation gains [1].

Table 1. Comparing the responses of the DBC system under the conditions of scenario 1.

	Scenario 1					
	Proposed Approach			The Method in Ref. [1]		
	$x_{1(t)}$	$x_{2(t)}$	$u(t)$	$x_{1(t)}$	$x_{2(t)}$	$u(t)$
Converge time	0.022	0.0194	0.0195	0.113	0.0817	0.153
Overshoot	0.031	0	0	0.33	1.87	0.01
Undershoot	0	0	0	0	0	0
Chattering	NO	NO	NO	NO	NO	YES

In addition, the sliding surface curve shown in Figure 5 shows that the sliding surface curve in the suggested method, compared to the reference [1], has less overshoot and undershoot. According to Figure 6, the adaptation gains have a very small slope and are absolute terms. Finally, the effectiveness and feasibility of the suggested control technique can be concluded from the simulation results.

Scenario 2. *In the next case, the system parameters are* $V_{in} = 12$ V, $V_{out} = 40$ V, *and* $R = 30$ *to* $50\ \Omega$. *In scenario 2, after setting the parameters, the results are obtained as follows. The DBC system state trajectory behaviour in scenario two is shown in Figure 7. Figure 8 depicts the control effort signals of the DBC system of the proposed method and the method in Ref. [1] under scenario 2. In Figure 9, the sliding surface under scenario 2 conditions are given. Figure 10 displays the adaptation gains curves under scenario 2.*

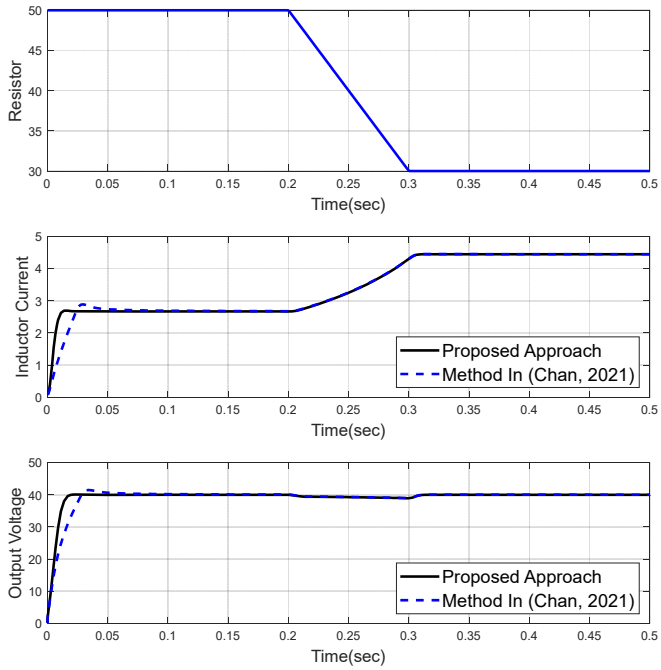

Figure 7. Comparison of the behaviour of the inductor current and output voltage with the results of the method in Ref. [1] in case of resistance changes.

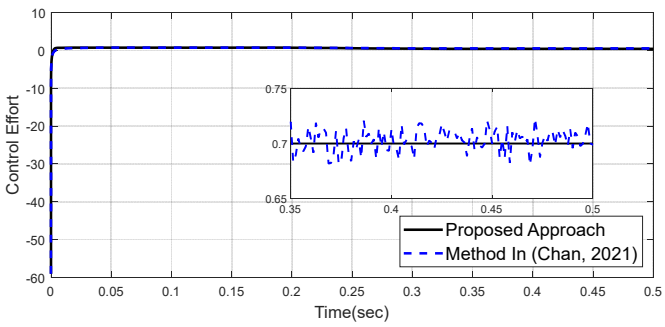

Figure 8. Controller effort signals [1].

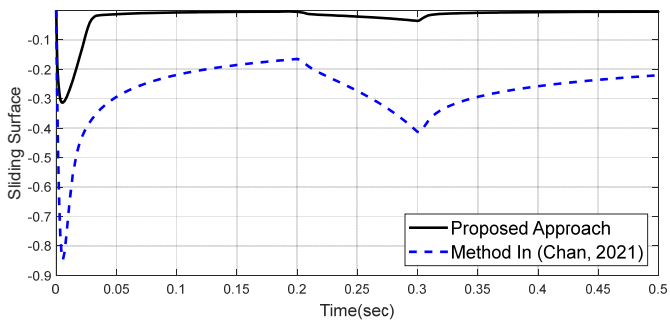

Figure 9. Sliding surfaces [1].

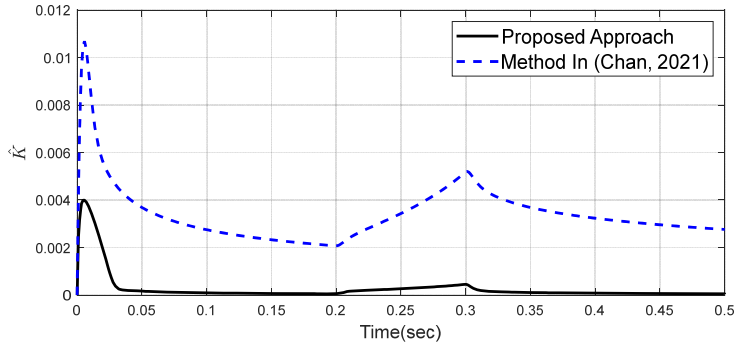

Figure 10. Adaptation gains [1].

From Figure 7 and Table 2, it can be concluded that the first state variable of the DBC system is stable after a finite time and has less overshoot and undershoot than the method in Ref. [1]. In addition, the second state trajectory converges to 40 V in a very short period and has less overshoot and undershoot compared to the method in Ref. [1]. Based on Table 2 and Figure 7, the control effort signal suggested approach completely eliminates the chattering problem and has better results in the steady state.

Table 2. Comparing the responses of the DBC system under the conditions of scenario 2.

	Scenario 2					
	Proposed Approach			The Method in Ref. [1]		
	$x_{1(t)}$	$x_{2(t)}$	$u(t)$	$x_{1(t)}$	$x_{2(t)}$	$u(t)$
Converge time	0.0137	0.0195	0.0116	0.05299	0.0672	0.02213
Overshoot	0	0	0	0.157	1.47	0
Undershoot	0	1	0	0	1	0
Chattering	NO	NO	NO	NO	NO	YES

Based on Figure 9, the switching surface curve in the suggested method has very few oscillations compared to the method in Ref. [1]. From Figure 10, the adaptation gains are absolute terms, and the disturbance estimation has a very small slope. According to the simulation results, it can be concluded that the proposed scheme has high effectiveness and is robust to external disturbances.

Scenario 3. *In the third step, the system parameters are considered to be* $V_{in} = 12$ *to* 20 V, $V_{out} = 40$ V, *and* $R = 30\ \Omega$. *In the third scenario, the simulation results are obtained after placing the parameters. The DBC system state trajectory behaviour in scenario 3 is shown in Figure 11. Figure 12 depicts the input control effort signals of the suggested method and the method in Ref. [1] under scenario 3.*

According to the obtained simulation results in Figures 11–14 and Table 3, it can be seen that the inductor current and output voltage of the DBC system are shown in Figure 11, which converges to the $\tilde{x}_1(t)$ after a short period of time; additionally, the suggested controller technique has less overshoot and undershoot compared to the method in Ref. [1]. According to Table 3 and Figure 12, the control effort signal in the suggested method completely eliminates the chattering problem and has better results. In Figure 13, the sliding surface signal in scenario three is given. Figure 14 displays the adaptation gain in scenario 3.

In addition, the switching surface curve shown in Figure 13 shows that the switching surface curve in the suggested method, compared to the reference [1] method, has less overshoot and undershoot. Ultimately, from Figure 14, the adaptation gains estimated the external disturbance with minimum slope. Simulation results demonstrate the effectiveness and feasibility of the suggested control technique in scenario 3.

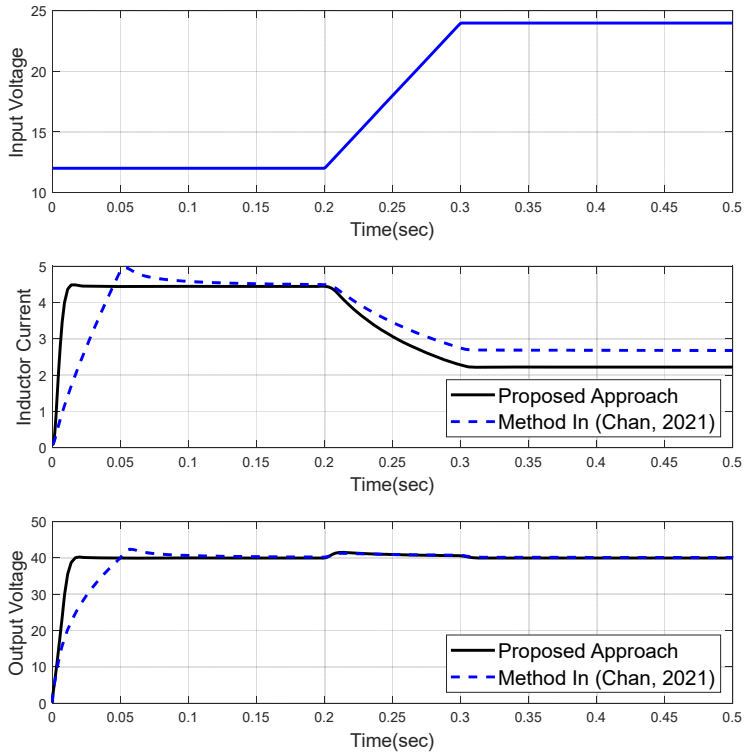

Figure 11. Comparison of the behaviour of the inductor current and output voltage with the results of the method in Ref. [1] in case of input voltage changes.

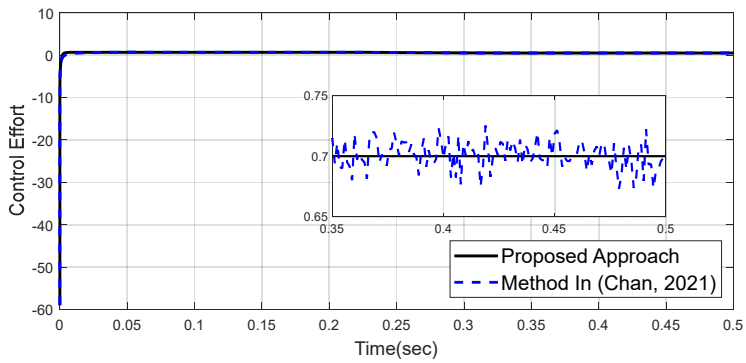

Figure 12. Controller effort signals [1].

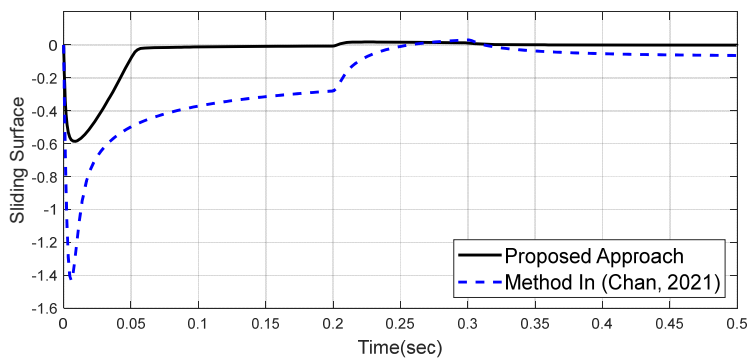

Figure 13. Sliding surfaces [1].

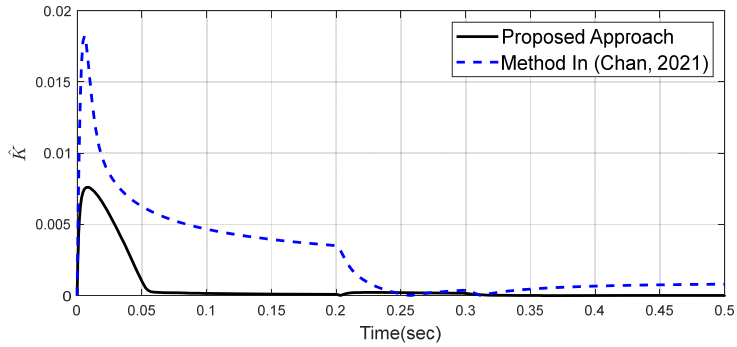

Figure 14. Adaptation gains [1].

Table 3. Comparing the responses of the DBC system under the conditions of scenario 3.

Scenario 3						
	Proposed Approach			The method in Ref. [1]		
	$x_{1(t)}$	$x_{2(t)}$	$u(t)$	$x_{1(t)}$	$x_{2(t)}$	$u(t)$
Converge time	0.02213	0.1787	0.0087	0.1302	0.09635	0.333
Overshoot	0.042	1.28	0	0.522	2.41	0
Undershoot	0	0	0	0	0	0
Chattering	NO	NO	NO	NO	NO	YES

Scenario 4. *In this scenario, the system parameters are considered to be* $V_{in} = 12$ V, $V_{out} = 40$ *to* 25 V, *and* $R = 30\ \Omega$. *In the final scenario, after placing the parameters in the control rule, the results are obtained as follows. The DBC system state trajectory behaviour is demonstrated in Figure 15. Figure 16 depicts the control effort signals of the DBC system of the proposed method and the method in Ref. [1] under scenario 4. Figure 17 shows the sliding surface, which has low oscillation. Figure 18 displays the adaptation gains curves under scenario 4 conditions.*

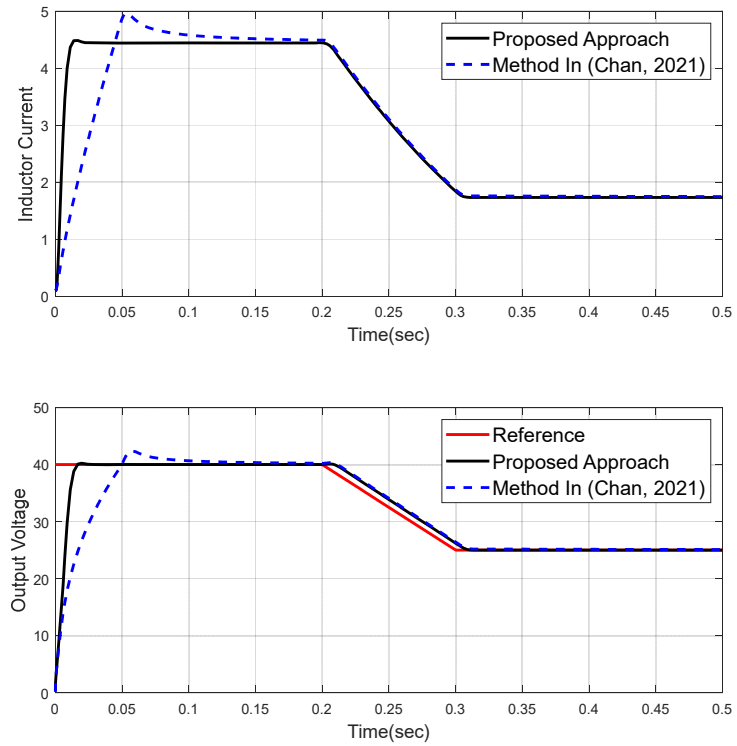

Figure 15. Comparison of the behaviour of the inductor current and output voltage with the results of the method in Ref. [1] in case of output voltage changes.

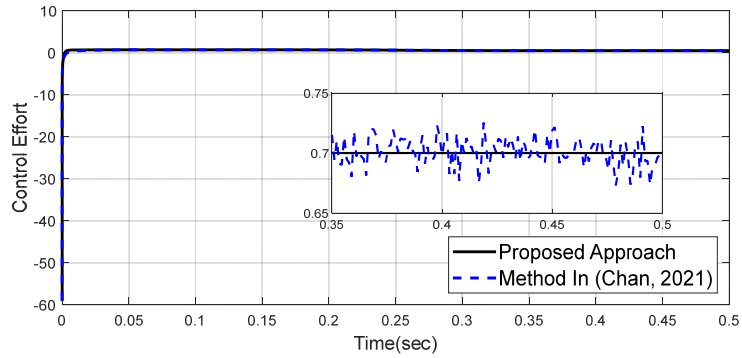

Figure 16. Controller effort signals [1].

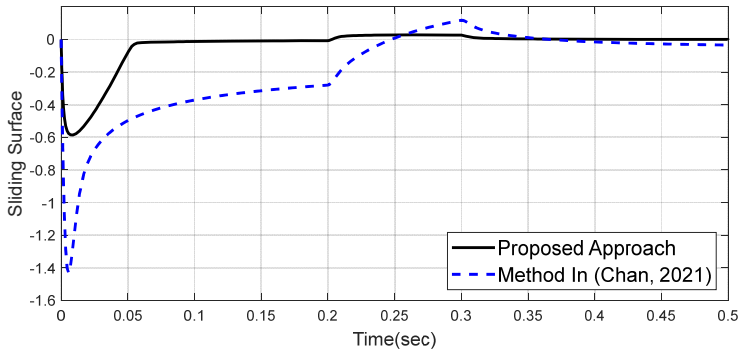

Figure 17. Sliding surfaces [1].

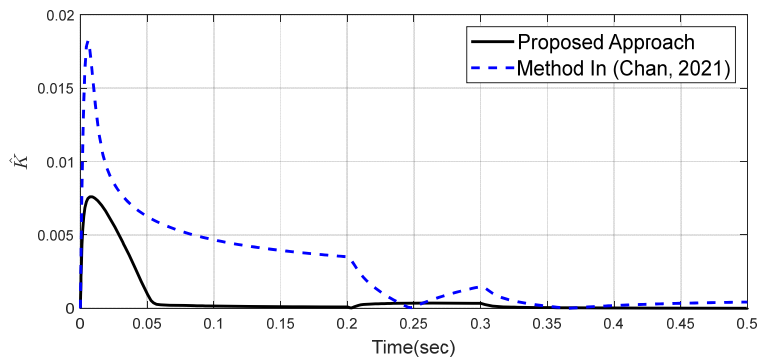

Figure 18. Adaptation gains [1].

It can be seen that the inductor current and output voltage of the DBC system are shown in Figure 15, which converges to the $\tilde{x}_1(t)$ after a short period of time; additionally, from Table 4, it is shown that the suggested controller technique has less undershoot and overshoot compared to the method in Ref. [1]. The chattering phenomenon in the control effort signal is eliminated in a steady state.

Table 4. Comparing the responses of the DBC system under the conditions of scenario 4.

	Scenario 4					
	Proposed Approach			The method in Ref. [1]		
	$x_{1(t)}$	$x_{2(t)}$	$u(t)$	$x_{1(t)}$	$x_{2(t)}$	$u(t)$
Converge time	0.02774	0.02511	0.0056	0.1321	0.113	0.02956
Overshoot	0.026	0.24	0	0. 511	2.41	0
Undershoot	0	0	0	0	0	0
Chattering	NO	NO	NO	NO	NO	YES

In addition, the sliding surface curve shown in Figure 17 shows that the sliding surface curve in the suggested method, compared to the reference Ref. [1] method, has less overshoot and undershoot. According to Figure 18, the adaptation gains are absolute terms, and the disturbance estimation has a very small slope.

Scenario 5. *In this scenario, the DBC system parameters are assumed as* $L = 220$ µH, $C = 470$ µF, $R = 80\,\Omega$, $V_{in} = 25$ V, *and* $V_{out} = 50$ V. *The external disturbance of the DBC system is considered by* $d(x_i(t), t) = \cos\left(\frac{3\pi t}{2}\right)$. *This scenario considers the effect of measurement noise on the DBC system. A zero-mean white noise with a noise power of 0.01 and a sample duration of 0.001 is added to the measurement, as demonstrated in Figure 19. Now, the responses of the DBC system are presented in terms of speed of convergence and robustness, as well as the elimination of the chattering phenomenon. Figure 20 demonstrates the behaviour of the inductor current and the output voltage, based on which the proposed controller performs well in terms of convergence rate and elimination of the chattering problem. The control effort signal is also displayed in Figure 21, demonstrating that the control input signals are smooth and have no chattering. Figure 22 shows the sliding surface, indicating that the control input's amplitude is appropriate. The adaptation gain is also demonstrated in Figure 23, based on which it can be seen that the external disturbances and white noise are well estimated by the proposed controller.*

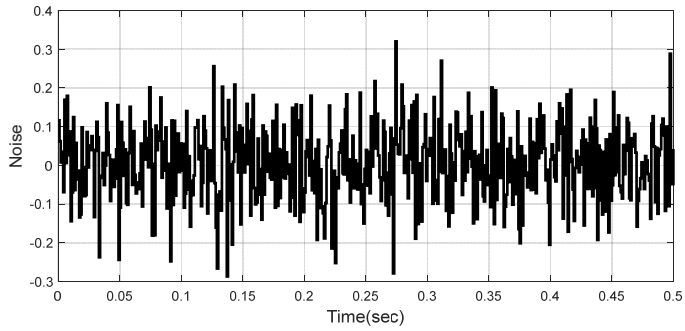

Figure 19. Measurement noise.

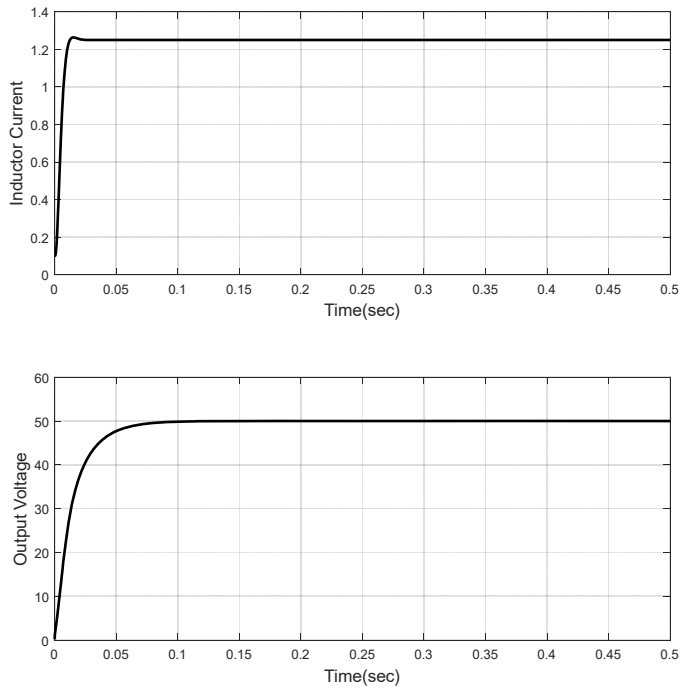

Figure 20. The behaviour of the inductor current and output voltage in the presence of measurement noise.

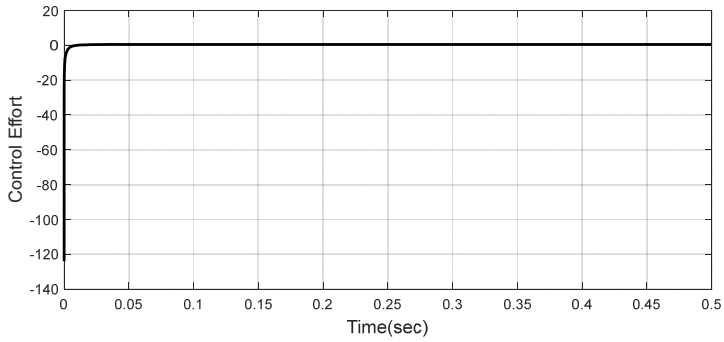

Figure 21. Controller effort signal in the presence of measurement noise.

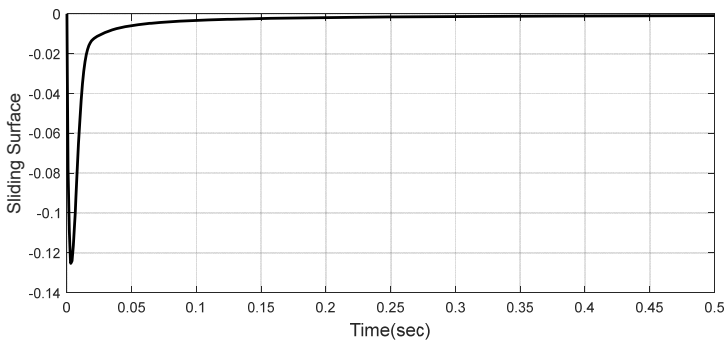

Figure 22. Sliding surface in the presence of measurement noise.

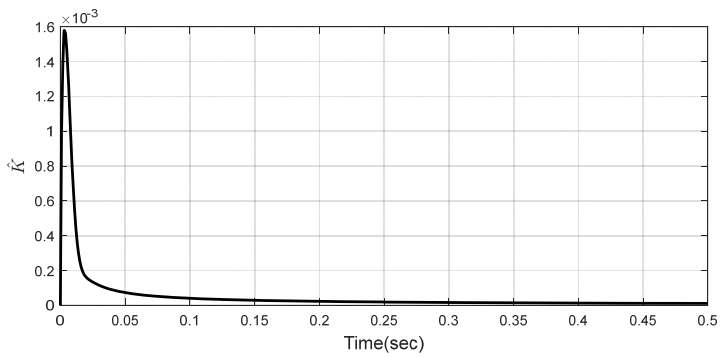

Figure 23. Adaptation gain.

According to Figure 20, it can be seen that the output voltage converges to 50 V without any overshoot or undershoot after a short time. In addition, it can be seen that the inductor current has become stable after about 0.02 s and has a very small overshoot. Based on Figure 21, the control effort signal is smooth and continuous and successfully eliminates the chattering phenomenon in the steady-state response.

In addition, the sliding surface curve shown in Figure 22 demonstrates that the sliding surface curve in the suggested method has a small overshoot and undershoot. According to Figure 23, the adaptation gains have a very small slope and are absolute terms. Finally, the effectiveness and feasibility of the suggested control technique can be concluded from the simulation results.

Scenario 6. *In the next case, the system parameters are* $L = 220$ μH, $C = 470$ μF, $V_{in} = 25$ V, $V_{out} = 50$ V, *and* $R = 80$ *to* $40\ \Omega$. *In scenario 6, after setting the parameters, the results are obtained as follows: The DBC system state trajectory behaviour in the presence of measurement noise is shown in Figure 24. Figure 25 depicts the control effort signals of the DBC system of the proposed method in the presence of measurement noise. In Figure 26, the sliding surface in the*

presence of measurement noise is given. Figure 27 displays the adaptation gain curve in the presence of measurement noise.

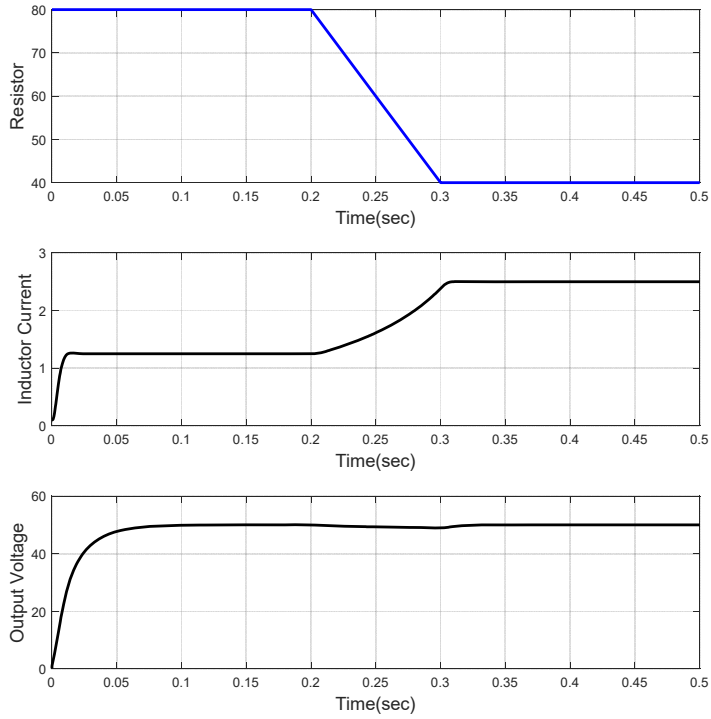

Figure 24. The behaviour of the inductor current and output voltage in the presence of measurement noise.

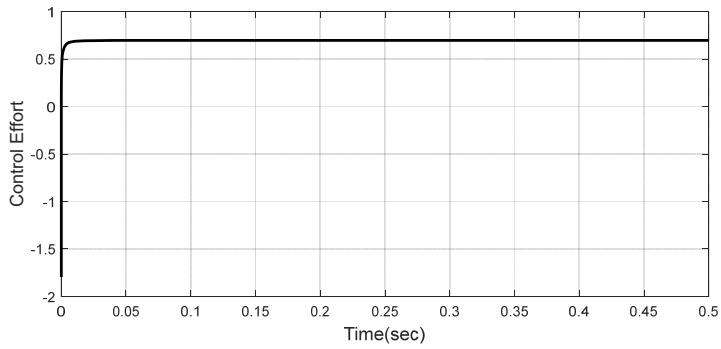

Figure 25. Controller effort signal in the presence of measurement noise.

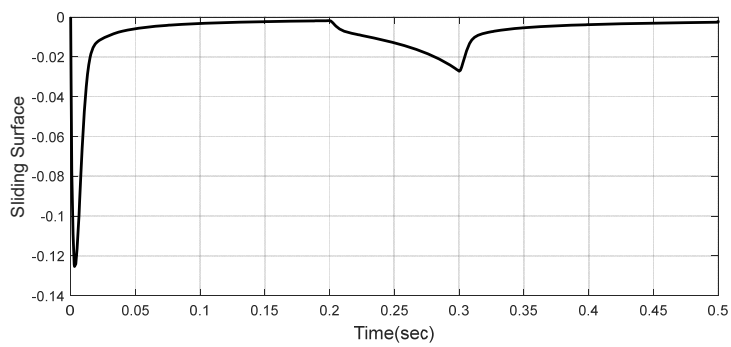

Figure 26. Sliding surface in the presence of measurement noise.

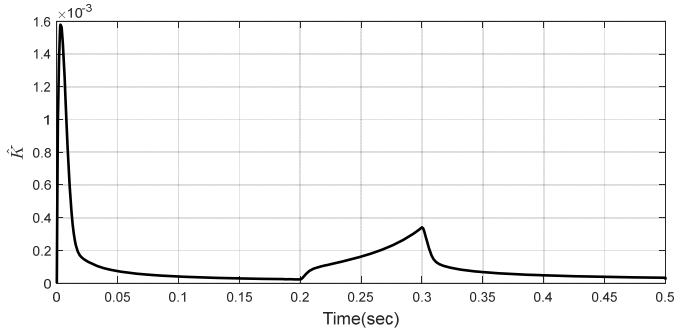

Figure 27. Adaptation gain.

From Figure 24, it can be concluded that the first state variable of the DBC system is stable after a finite time and has a small overshoot and undershoot in the presence of measurement noise. In addition, the second state trajectory converges to 50 V in a very short period and has a small overshoot. Based on Figure 25, the suggested control effort signal completely eliminates the chattering problem and has acceptable results in the steady state.

Based on Figure 26, the switching surface curve in the suggested method has very small oscillations. From Figure 27, the adaptation gain is an absolute term; the disturbance and white noise estimation have a very small slope. According to the simulation results, it can be concluded that the proposed scheme has high effectiveness and is robust to external disturbances and white noise.

Scenario 7. *In the seventh step, the system parameters are considered to be* $L = 220$ μH, $C = 470$ μF, $V_{in} = 12$ *to* 25 V, $V_{out} = 50$ V, *and* $R = 80\ \Omega$. *In the seventh scenario, the simulation results are obtained after placing the parameters. The DBC system state trajectory behaviour in the seventh scenario is shown in Figure 28. Figure 29 depicts the input control effort signals of the suggested method under scenario 7.*

Based on Figure 28, it can be seen that the output voltage value of the disturbed DBC system converges to 50 V in a finite time. Furthermore, it can be seen that the output voltage value of the disturbed DBC system remains stable in the presence of an increase in the input voltage from 12 to 25 V with a decrease in the inductor current. Figure 29 indicates the control effort signal obtained in the presence of external disturbances and white noise, which is smooth and continuous and has well eliminated the chattering phenomenon in the steady-state response. In Figure 30, the sliding surface signal in seventh scenario is given. Figure 31 demonstrate the adaptation gain in scenario 7.

In addition, the switching surface curve shown in Figure 30 shows that the switching surface curve in the suggested method has a small overshoot and undershoot. Ultimately, from Figure 31, the adaptation gain estimates the external disturbance and white noise with minimum slope. Simulation results demonstrate the effectiveness and feasibility of the suggested control technique.

Scenario 8. *In the final scenario, the system parameters are considered to be* $L = 220$ μH, $C = 470$ μF, $V_{in} = 25$ V, $V_{out} = 50$ *to* 25 V, *and* $R = 80\ \Omega$. *In the final scenario, after placing the parameters in the control law, the results are obtained as follows. The DBC system state trajectory behaviour is demonstrated in Figure 32. Figure 33 depicts the control effort signal of the DBC system of the proposed method in the presence of measurement noise. Figure 34 shows the sliding surface, which has low oscillation. Figure 35 displays the adaptation gain curve in the presence of measurement noise.*

From Figure 32, it can be seen that the output voltage converges to the reference value in a finite time with low oscillations. Furthermore, it can be seen that the inductor current is sensitive to changes in the output voltage and is reduced with a decrease in the output voltage. Based on Figure 33, few control efforts have been made to trace the trajectories of the disturbed DBC system and the obtained control signal has a smooth and continuous steady-state response.

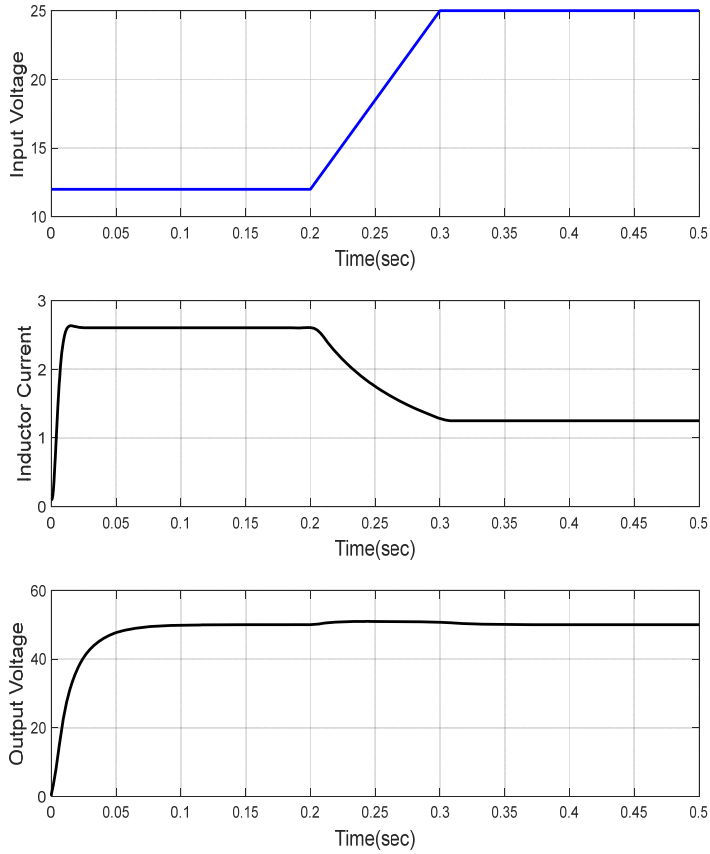

Figure 28. The behaviour of the inductor current and output voltage in case of input voltage changes and in the presence of measurement noise.

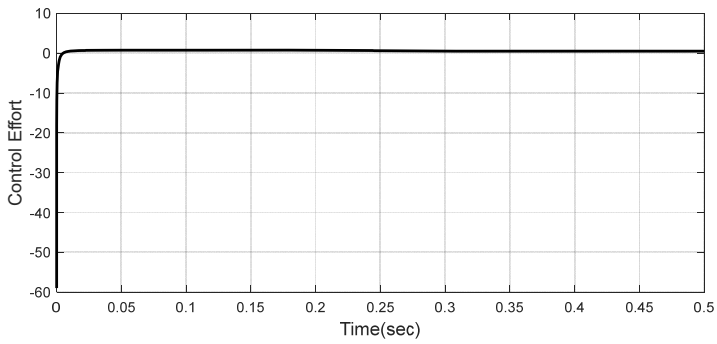

Figure 29. Control effort signal in the presence of measurement noise.

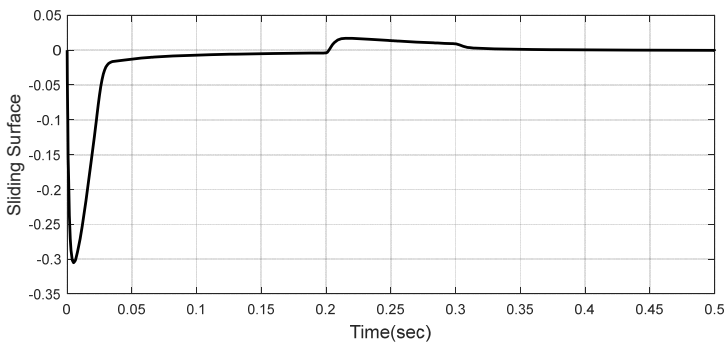

Figure 30. Sliding surface in the presence of measurement noise.

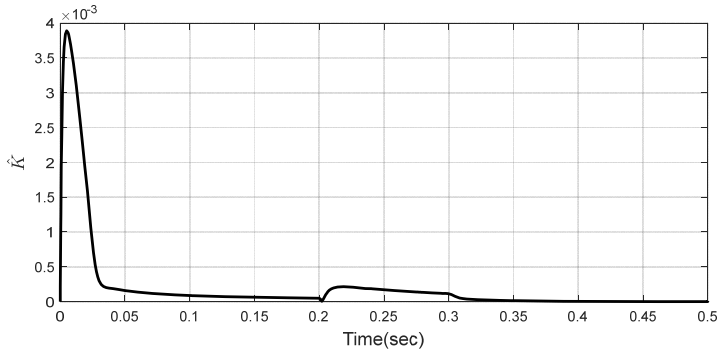

Figure 31. Adaptation gain.

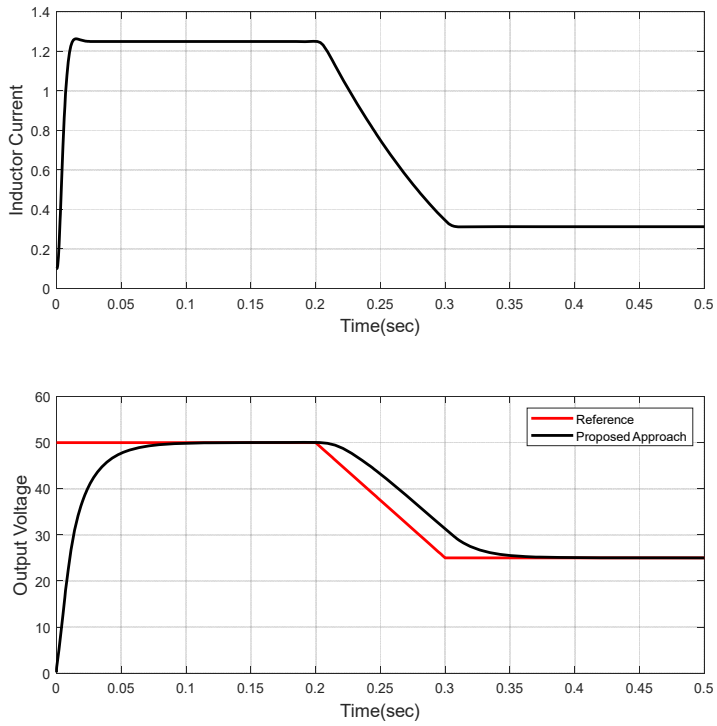

Figure 32. The behaviour of the inductor current and output voltage in case of output voltage changes and in the presence of measurement noise.

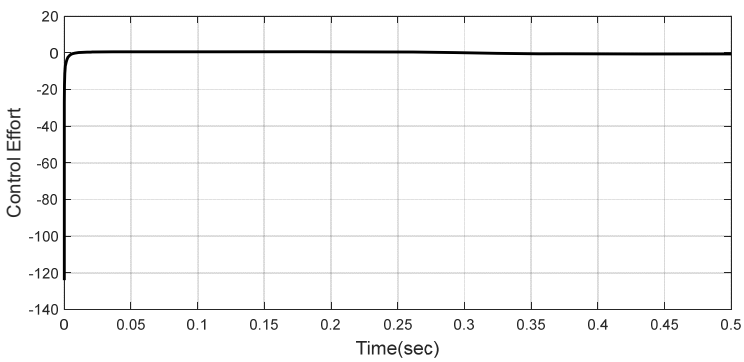

Figure 33. Controller effort signal in the presence of measurement noise.

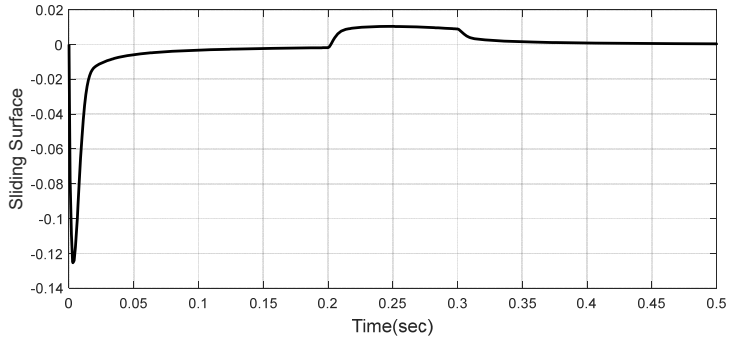

Figure 34. Sliding surface in the presence of measurement noise.

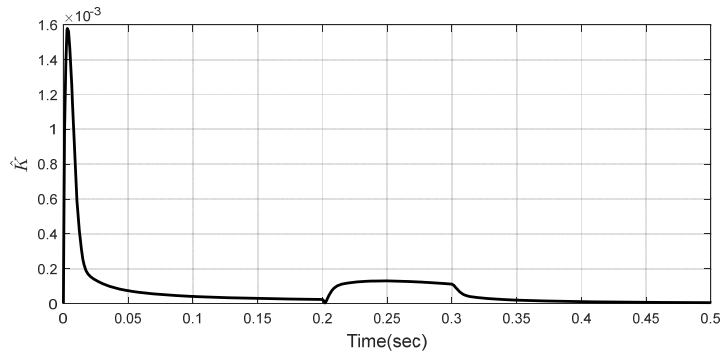

Figure 35. Adaptation gain.

Furthermore, the sliding surface curve shown in Figure 34 illustrates that the sliding surface curve in the suggested method has a small overshoot and undershoot. According to Figure 35, the adaptation gain is an absolute term, and the disturbance estimation has a very small slope. According to the simulation results, it can be concluded that the proposed scheme has high effectiveness and is robust to external disturbances and white noise. The simulation results in scenario 8 confirm the effectiveness of the suggested control method to control the DBC system under disturbance and demonstrate that in all scenarios, the presented control scheme successfully eliminates the chattering phenomenon, a continuous and smooth control signal is obtained, and the state trajectories of DBC system converge to the reference signal in a finite time.

5. Conclusions

In this paper, using the Lyapunov stability theory and adaptive control approach, a TSMC for DBC systems with unknown disturbances was presented. The discontinuity in the control rules, which is the main weakness of the conventional SMC, is eliminated by using this method. In addition, the estimation of the unknown boundaries of external disturbances is performed continuously using a novel adaptive control law. The simulations showed that the proposed finite-time controller could provide a fast and favourable response and weaken and eliminate the umbrella phenomenon well. It was also observed that the output of the closed-loop system under control is robust to load and input voltage changes and the closed-loop system is guaranteed to be asymptotically stable. This control scheme can be extended for future work on buck and buck–boost converters.

Author Contributions: Conceptualization, H.A., K.-H.H. and E.M.A.; formal analysis, M.A.S., E.M.A. and S.M.; funding acquisition, H.A., E.M.A. and A.A.; investigation, K.-H.H., A.A. and S.M.; methodology, S.M. and M.A.S.; writing—original draft, M.A.S., H.A. and S.M.; writing—review and editing K.-H.H., E.M.A. and A.A.; supervision, S.M., A.A. and K.-H.H. All authors have read and agreed to the published version of the manuscript.

Funding: The authors extend their appreciation to the Deputyship for Research & Innovation, Ministry of Education in Saudi Arabia for funding this research work through the project number 223202.

Institutional Review Board Statement: Not applicable.

Informed Consent Statement: Not applicable.

Data Availability Statement: The data that support the findings of this study are available within the article.

Conflicts of Interest: The authors declare no conflict of interest.

Nomenclature

S_ω	Switch	$\tilde{x}(t)$	Reference signal
D	Fast diode	$e(t)$	Error signal
R	Resistance	$\tau(t)$	Sliding surface
L	Inductor	ρ	Positive and constant parameter
C	Capacitor	η	Positive parameter
u	Control input	σ	Positive parameter
$\dot{I}_L$	Inductor current	z	Positive odd integer
V_C	Capacitor voltage	s	Positive odd integer with condition $z > s$
V_{in}	Input voltage	b	Positive odd integer
V_{out}	Output voltage	V	The candidate Lyapunov's function
t_0	Initial time	μ	Positive constant
t_s	Settling time	α	Changes in the sliding surface
$x_i(t)$	Converter state	φ	Constant coefficient
d_i	External disturbances	D	Unknown upper bounds of external disturbances
σ_i	Scalar value	$\hat{D}$	Estimation of D

References

1. Chan, C.-Y. Adaptive sliding-mode control of a novel buck-boost converter based on Zeta converter. *IEEE Trans. Circuits Syst. II Express Briefs* **2021**, *69*, 1307–1311. [CrossRef]
2. Shen, L.; Lu, D.D.C.; Li, C. Adaptive sliding mode control method for DC–DC converters. *IET Power Electron.* **2015**, *8*, 1723–1732. [CrossRef]
3. Hirsch, A.; Parag, Y.; Guerrero, J. Microgrids: A review of technologies, key drivers, and outstanding issues. *Renew. Sustain. Energy Rev.* **2018**, *90*, 402–411. [CrossRef]
4. Lin, S.-Y.; Chen, J.-F. Distributed optimal power flow for smart grid transmission system with renewable energy sources. *Energy* **2013**, *56*, 184–192. [CrossRef]
5. Sun, G.; Chen, S.; Wei, Z.; Chen, S. Multi-period integrated natural gas and electric power system probabilistic optimal power flow incorporating power-to-gas units. *J. Mod. Power Syst. Clean Energy* **2017**, *5*, 412–423. [CrossRef]
6. Borlase, S. *Smart Grids: Infrastructure, Technology, and Solutions*; CRC Press: Boca Raton, FL, USA, 2017.
7. Sinvula, R.; Abo-Al-Ez, K.M.; Kahn, M.T. Harmonic source detection methods: A systematic literature review. *IEEE Access* **2019**, *7*, 74283–74299. [CrossRef]
8. Hatahet, W.; Marei, M.I.; Mokhtar, M. Adaptive controllers for grid-connected DC microgrids. *Int. J. Electr. Power Energy Syst.* **2021**, *130*, 106917. [CrossRef]
9. Rana, N.; Banerjee, S. Development of an improved input-parallel output-series buck-boost converter and its closed-loop control. *IEEE Trans. Ind. Electron.* **2019**, *67*, 6428–6438. [CrossRef]
10. Alajmi, B.N.; Marei, M.I.; Abdelsalam, I.; Ahmed, N.A. Multiphase Interleaved Converter Based on Cascaded Non-Inverting Buck-Boost Converter. *IEEE Access* **2022**, *10*, 42497–42506. [CrossRef]
11. Zhang, Y.; Liu, H.; Li, J.; Sumner, M.; Xia, C. DC–DC boost converter with a wide input range and high voltage gain for fuel cell vehicles. *IEEE Trans. Power Electron.* **2018**, *34*, 4100–4111. [CrossRef]
12. Özdemir, A.; Erdem, Z. Double-loop PI controller design of the DC-DC boost converter with a proposed approach for calculation of the controller parameters. *Proc. Inst. Mech. Eng. Part I J. Syst. Control Eng.* **2018**, *232*, 137–148. [CrossRef]
13. Kobaku, T.; Jeyasenthil, R.; Sahoo, S.; Ramchand, R.; Dragicevic, T. Quantitative feedback design-based robust PID control of voltage mode controlled DC-DC boost converter. *IEEE Trans. Circuits Syst. II Express Briefs* **2020**, *68*, 286–290. [CrossRef]
14. Yanarates, C.; Zhou, Z. Design and Cascade PI Controller-Based Robust Model Reference Adaptive Control of DC-DC Boost Converter. *IEEE Access* **2022**, *10*, 44909–44922. [CrossRef]

15. Kazimierczuk, M.K.; Massarini, A. Feedforward control of DC-DC PWM boost converter. *IEEE Trans. Circuits Syst. I Fundam. Theory Appl.* **1997**, *44*, 143–148. [CrossRef]
16. Chen, H.-C.; Lan, Y.-C. Unequal Duty-Ratio Feedforward Control to Extend Balanced-Currents Input Voltage Range for Series-Capacitor-Based Boost PFC Converter. *IEEE Trans. Ind. Electron.* **2022**, *70*, 4289–4292. [CrossRef]
17. Adnan, M.F.; Oninda, M.A.M.; Nishat, M.M.; Islam, N. Design and simulation of a dc-dc boost converter with pid controller for enhanced performance. *Int. J. Eng. Res. Technol. (IJERT)* **2017**, *6*, 27–32.
18. Ghazali, M.R.; Ahmad, M.A.; Suid, M.H.; Tumari, M.Z.M. A DC/DC Buck-Boost Converter-Inverter-DC Motor Control based on model-free PID Controller tuning by Adaptive Safe Experimentation Dynamics Algorithm. In Proceedings of the 2022 57th International Universities Power Engineering Conference (UPEC), Istanbul, Turkey, 30 August–2 September 2022; pp. 1–6.
19. Karamanakos, P.; Geyer, T.; Manias, S. Direct voltage control of DC–DC boost converters using enumeration-based model predictive control. *IEEE Trans. Power Electron.* **2013**, *29*, 968–978. [CrossRef]
20. Ullah, B.; Ullah, H.; Khalid, S. Direct Model Predictive Control of Noninverting Buck-boost DC-DC Converter. *CES Trans. Electr. Mach. Syst.* **2022**, *6*, 332–339. [CrossRef]
21. Gupta, T.; Boudreaux, R.; Nelms, R.M.; Hung, J.Y. Implementation of a fuzzy controller for DC-DC converters using an inexpensive 8-b microcontroller. *IEEE Trans. Ind. Electron.* **1997**, *44*, 661–669. [CrossRef]
22. So, W.-C.; Tse, C.K.; Lee, Y.-S. A fuzzy controller for DC-DC converters. In Proceedings of the 1994 Power Electronics Specialist Conference-PESC'94, Taipei, Taiwan, 20–25 June 1994; pp. 315–320.
23. Beccuti, A.G.; Papafotiou, G.; Morari, M. Optimal control of the boost dc-dc converter. In Proceedings of the 44th IEEE Conference on Decision and Control, Seville, Spain, 12–15 December 2005; pp. 4457–4462.
24. Mitra, L.; Rout, U.K. Optimal control of a high gain DC-DC converter. *Int. J. Power Electron. Drive Syst.* **2022**, *13*, 256. [CrossRef]
25. Kahani, R.; Jamil, M.; Iqbal, M.T. Direct Model Reference Adaptive Control of a Boost Converter for Voltage Regulation in Microgrids. *Energies* **2022**, *15*, 5080. [CrossRef]
26. Jeong, G.-J.; Kim, I.-H.; Son, Y.-I. Application of simple adaptive control to a dc/dc boost converter with load variation. In Proceedings of the 2009 ICCAS-SICE, Fukuoka, Japan, 18–21 August 2009; pp. 1747–1751.
27. Guldemir, H. Sliding mode control of DC-DC boost converter. *J. Appl. Sci.* **2005**, *5*, 588–592. [CrossRef]
28. Utkin, V. Sliding mode control of DC/DC converters. *J. Frankl. Inst.* **2013**, *350*, 2146–2165. [CrossRef]
29. Wang, J.; Rong, J.; Yu, L. Dynamic prescribed performance sliding mode control for DC–DC buck converter system with mismatched time-varying disturbances. *ISA Trans.* **2022**, *129*, 546–557. [CrossRef]
30. Wai, R.-J.; Shih, L.-C. Adaptive fuzzy-neural-network design for voltage tracking control of a DC–DC boost converter. *IEEE Trans. Power Electron.* **2011**, *27*, 2104–2115. [CrossRef]
31. Wang, Y.-X.; Yu, D.-H.; Kim, Y.-B. Robust time-delay control for the DC–DC boost converter. *IEEE Trans. Ind. Electron.* **2013**, *61*, 4829–4837. [CrossRef]
32. Rojsiraphisal, T.; Mobayen, S.; Asad, J.H.; Vu, M.T.; Chang, A.; Puangmalai, J. Fast terminal sliding control of underactuated robotic systems based on disturbance observer with experimental validation. *Mathematics* **2021**, *9*, 1935. [CrossRef]
33. Ghadiri, H.; Khodadadi, H.; Mobayen, S.; Asad, J.H.; Rojsiraphisal, T.; Chang, A. Observer-based robust control method for switched neutral systems in the presence of interval time-varying delays. *Mathematics* **2021**, *9*, 2473. [CrossRef]
34. Sarkar, T.T.; Mahanta, C. Estimation Based Sliding Mode Control of DC-DC Boost Converters. *IFAC-PapersOnLine* **2022**, *55*, 467–472. [CrossRef]
35. Sepestanaki, M.A.; Jalilvand, A.; Mobayen, S.; Zhang, C. Design of adaptive continuous barrier function finite time stabilizer for TLP systems in floating offshore wind turbines. *Ocean Eng.* **2022**, *262*, 112267. [CrossRef]
36. Utkin, V. Discussion aspects of high-order sliding mode control. *IEEE Trans. Autom. Control* **2015**, *61*, 829–833. [CrossRef]
37. Liu, X.; Han, Y.; Wang, C. Second-order sliding mode control for power optimisation of DFIG-based variable speed wind turbine. *IET Renew. Power Gener.* **2017**, *11*, 408–418. [CrossRef]
38. Liu, X.; Han, Y. Decentralized multi-machine power system excitation control using continuous higher-order sliding mode technique. *Int. J. Electr. Power Energy Syst.* **2016**, *82*, 76–86. [CrossRef]
39. RakhtAla, S.M.; Yasoubi, M.; HosseinNia, H. Design of second order sliding mode and sliding mode algorithms: A practical insight to DC-DC buck converter. *IEEE/CAA J. Autom. Sin.* **2017**, *4*, 483–497. [CrossRef]
40. Ma, R.; Wu, Y.; Breaz, E.; Huangfu, Y.; Briois, P.; Gao, F. High-order sliding mode control of DC-DC converter for PEM fuel cell applications. In Proceedings of the 2018 IEEE Industry Applications Society Annual Meeting (IAS), Portland, OR, USA, 23–27 September 2018; pp. 1–7.
41. Xiu, C.; Guo, P. Global terminal sliding mode control with the quick reaching law and its application. *IEEE Access* **2018**, *6*, 49793–49800. [CrossRef]
42. Ahmed, S.; Wang, H.; Tian, Y. Adaptive fractional high-order terminal sliding mode control for nonlinear robotic manipulator under alternating loads. *Asian J. Control* **2021**, *23*, 1900–1910. [CrossRef]
43. Yang, L.; Yang, J. Robust finite-time convergence of chaotic systems via adaptive terminal sliding mode scheme. *Commun. Nonlinear Sci. Numer. Simul.* **2011**, *16*, 2405–2413. [CrossRef]

44. Yao, Q. Fixed-time trajectory tracking control for unmanned surface vessels in the presence of model uncertainties and external disturbances. *Int. J. Control* **2022**, *95*, 1133–1143. [CrossRef]
45. Aghababa, M.P. Finite-time chaos control and synchronization of fractional-order nonautonomous chaotic (hyperchaotic) systems using fractional nonsingular terminal sliding mode technique. *Nonlinear Dyn.* **2012**, *69*, 247–261. [CrossRef]

Disclaimer/Publisher's Note: The statements, opinions and data contained in all publications are solely those of the individual author(s) and contributor(s) and not of MDPI and/or the editor(s). MDPI and/or the editor(s) disclaim responsibility for any injury to people or property resulting from any ideas, methods, instructions or products referred to in the content.